Paper No.
09207

NACE INTERNATIONAL CORROSION 2009 CONFERENCE & EXPO

CORROSION OF EPOXY- AND POLYMER/ZINC- COATED REBAR IN SIMULATED CONCRETE PORE SOLUTION

Kingsley Lau and Alberto A. Sagüés
Dept. of Civil and Environmental Engineering, University of South Florida
4202 E. Fowler Ave. ENB118, Tampa, FL 33620

ABSTRACT

This work is a preliminary examination of mechanistic issues on the comparative corrosion performance of regular epoxy-coated rebar (ECR) and dual polymer-zinc coated reinforcement (DCR) in simulated concrete pore solution with and without chloride ions, at polarizations from +100 mV to -1000 mV in the saturated calomel electrode (SCE) scale and exposure periods of 1 month or longer. Both materials had intentional coating breaks exposing the base steel. Polymer adhesion degradation of DCR relative to the as-received condition was comparable to, or less than, that experienced by ECR under both anodic and cathodic polarization and with and without chloride ions. Both DCR and ECR experienced severe corrosion at breaks under strong anodic polarization with chloride ions, but distress for DCR was significantly less than for ECR. Under open circuit conditions DCR experienced an initial high activity period both in the presence and absence of chloride ions after which the open circuit potential stabilized to ~-400 mV_{SCE}, and the exposed steel remained free of corrosion in either environment. In contrast, ECR in the presence of chlorides developed more negative open circuit potential (OCP) and visible corrosion. After the initial period of high activity, OCP consumption of the zinc exposed at the defect rim proceeded at a very low rate both in the presence or absence of chloride ions. In the absence of chloride ions and under medium to strong cathodic polarization, DCR showed cathodic current (and hence an ability to support corrosion macrocells with through-the-steel defects) no greater than that for ECR.

Keywords: epoxy, zinc, dual-coat, disbondment, rebar, corrosion

INTRODUCTION

Epoxy-coated rebar (ECR) has been used for over 30 years as means of corrosion control for reinforced concrete structures exposed to chloride environments, yet varying corrosion performance has been reported in field and laboratory examinations[1-10]. ECR has been used mainly with success in bridge decks exposed primarily and intermittently to deicing salts. In contrast, poor corrosion performance, where severe corrosion had occurred after only a few years after service, has been observed in structures in marine environments.

New methods intended to improve corrosion durability of ECR, such as dual polymer-zinc coated reinforcement (DCR), are being assessed[11-14]. DCR contains a thin layer of nearly pure zinc less than 0.05 mm thick applied by thermal spraying to the steel surface prior to an epoxy polymer coating ~0.2 mm. Initial results of ongoing research on mechanistic issues on the corrosion resistance of DCR comparatively examined with ECR in simulated concrete pore solution are presented. The ultimate objectives of the investigation are to assess the stability of the polymer to zinc/steel substrate bond, gauge the potential severity of crevice corrosion, determine the extent of cathodic reaction (relevant to possible corrosion macrocell intensity), and determine the extent of beneficial galvanic action that the zinc coating may provide.

EXPERIMENTAL PROCEDURE

DCR and ECR (1.6 cm diameter) test samples were prepared from stock provided by a manufacturer of both products. Initial assessments of sample quality including coating thickness measured by magnetic gage readings, coating quality (in terms of presence of holidays or mechanical coating damage) and zinc layer thickness of DCR determined by metallographic examination were made. Sample bar lengths (23 cm) that were free of mechanically-induced coating defects were cut out, and intentional coating defects were introduced by drilling to the steel substrate with a 1.6 mm diameter drill bit to a nominal depth from the coating outer surface to the tip of the drill cavity of 1 mm. Defect locations were located in bar areas between adjacent deformation ribs, Figure 1. Total exposed steel area was ~0.45cm^2. The two cut ends of the bar samples were coated with epoxy patch compounds for DCR or ECR provided by the bar manufacturer. The bottom 1.9 cm of the bar was set in metallographic epoxy to cap the bottom end of the bar to prevent corrosion there, and to serve as a base stand for the sample. A stainless steel set screw was tapped on to the top end for electrical connection.

Electrochemical Tests

DCR and ECR were tested in two simulated concrete pore solution (SPS) environments; one containing 3.5 wt% (0.6M) NaCl and the other without NaCl addition. Solution constituents and pH are listed in Table 1. The bar samples were partially immersed (19 cm length (~95 cm^2 surface area) in contact with liquid) in each solution with the set screw ~2 cm above water. Test chambers were sealed to avoid solution carbonation with atmospheric CO_2 but leaving enough air volume to avoid any significant O_2 depletion during the tests. Solution temperature was 22 ± 2 ^{o}C.

For the main sequence of tests, four polarization regimes, maintained with a multi-potentiostat, were used for each test group: +100 mV, -500 mV, -1000 mV, and open circuit potential (OCP), all measured with a saturated calomel electrode (SCE). An activated titanium mesh was used as a common counter electrode for each chamber and an activated titanium rod was used as a common reference electrode calibrated periodically with the SCE. The polarization potentials were maintained within ±5 mV of the desired value. The time of test for each specimen ranged from 33 to 52 days as listed in Table 2. All conditions were tested in duplicate.

In addition to the main test sequence, supplemental duplicate DCR specimens were made and placed for long term exposure and detailed evaluation in the OCP condition in both solutions. Results from the first ~50 days of exposure are reported here for those specimens, with continual monitoring in progress. Electrical potential and electrochemical impedance spectroscopy (EIS) measurements for nominal corrosion rate estimation were made at various times for all OCP specimens.

Post-exposure Examination

After exposure time per Table 2 was completed, the bar samples were removed and the extent of external corrosion and coating condition was assessed. The pH of moisture retained at the drilled defect cavities and, if present, in nearby disbonded regions was measured with pH paper.

Coating disbondment was measured by three methods including: disbondment radial length from the defect site perimeter, qualitative adhesion level for the region up to ~1 cm radial distance around the defect site, and pull-off strength at a spot adjacent to defect site. As it will be noted in the Results section, the mechanical characteristics of the thermally sprayed zinc layer necessitate special consideration in the interpretation of results from these tests.

The disbondment radial length was measured following a procedure similar to that in Ref 15 by cutting a 3mm wide strip in the area of bar between adjacent deformation ribs and another 3mm wide strip along the longitudinal axis of the bar centered on the defect site forming a skewed cross (Figure 2). The coating was cut to the steel substrate with a sharp thin blade. A small flap was peeled with the tip of the blade at one of the intersecting lines of the two strips and the strip was peeled back with tweezers until the cohesive strength was overcome and the applied force tore the strip from the bar. The distance from the tear point to the edge of the defect was recorded as the disbondment radial length. Four radial length measurements were made per selected defect site. The lengths measured for the entire bar were then averaged and reported.

The qualitative evaluation of the coating adhesion level used a four point scale as listed in Table 3. Sections of the strip (adjacent to defect site) between deformation ribs that were peeled during the disbondment radial length measurements were given a rating of 1 or 2 depending on ease of separation. The remaining portions, if present, of the strip up to 1 cm from the defect were cut into 3 mm segments. Each segment was evaluated per Table 3 and the average of all segments for all the defects examined in each bar was reported as the qualitative adhesion level of the bar. The pull-off strength was measured with a mechanical pull-off device[16]. A metal dolly (6 mm diameter) contoured to the surface curvature of bar between deformation ribs (radius ~1.6 cm) was attached with a cyanoacrylate adhesive to the outer polymer surface (lightly roughened and degreased) directly adjacent to the defect location. The polymer coating on the perimeter of the dolly was removed with a rotating dental drill bit. The dolly was then pulled until separation using a gimbal joint fixture to avoid shear stresses. The strength was recorded as the pull-off force divided by the nominal dolly area.

Visual observations of undercoating metal appearance were recorded. The pH of undercoating moisture if present was measured. The zinc layer immediate to defect locations was observed with an optical microscope. Two defect locations per bar test sample were cut transversely with a slow speed diamond saw with the edge centered on the defect site. The cross section was mounted in metallographic resin, ground and polished for microstructural assessment. For DCR samples, water free metallographic preparation procedures were followed to prevent artifact zinc corrosion.

RESULTS AND DISCUSSION

Initial and Visual Observations

The average polymer (or polymer plus zinc) coating thickness for ECR and DCR test samples was ~0.26mm and ~0.23mm, respectively (Figure 3). The average thickness of the zinc layer in DCR as determined metallographically was ~0.028mm. The standard deviation of the zinc layer thickness was

~0.01mm. These values are consistent with target production values for each material. It is noted that metallographic determination of zinc coating thickness tends to yield a value smaller than that obtained by magnetic gages as natural surface roughness increases the values reported by the latter method.

No formation of white zinc corrosion products on DCR was observed in any polarization regimes in either chloride or chloride-free solutions. In SPS solution in the absence of chloride ions, no physical observation of steel corrosion initiation was observed in any polarization regimes for ECR or DCR for the entirety of the test exposure. Bright metal luster was retained in all polarization regimes except for slight discoloration from incipient electrodeposition on exposed metal surfaces on ECR and DCR polarized -1000mV_{SCE}. In the presence of 3.5wt% NaCl, external corrosion products in the form of brown-red non-soluble tubercles developed at defect sites on DCR samples polarized +100mV_{SCE} and ECR samples polarized +100mV_{SCE}, -500mV_{SCE}, and OCP. The corrosion products developed on ECR and DCR samples polarized +100mV_{SCE} in less than 1 hour and after 2 days for ECR samples polarized at -500mV_{SCE}. Vestigial amounts of corrosion products were observed in ECR OCP samples after approximately 30 days. On ECR samples polarized +100mV_{SCE} and -500mV_{SCE}, external corrosion products developed also away from (but within the vicinity of) intentional defect sites. The corrosion there was due to blistering and subsequent cracking of the polymer coating from tensile stresses caused by accumulation of internal corrosion product by intentional defect sites. Slight swelling of the polymer coating around defect sites was observed on anodically polarized DCR but much less than on ECR and without cracking of polymer coating. Bright metal luster in the defect cavity was mostly retained for ECR and DCR in the other polarization regimes; slight discoloration similar to that observed in chloride-free solution on the exposed steel surface was observed in the -1000mV_{SCE} regime for both ECR and DCR.

Electrochemical Measurements

Open-Circuit Potential Evolution. The OCP of ECR in SPS solution was ~-200mV_{SCE} throughout the test period indicative of passive behavior and consistent with the absence of corrosion development (Figure 4). The OCP of ECR in chloride rich environment quickly reached ~-600mV_{SCE} indicative of corrosion activation consistent with high chloride concentrations ($[Cl^-]/[OH^-]$~2). Notably, the OCP of DCR evolved similarly in both chloride and chloride-free solution. In both solutions the OCP was ~-1200 mV_{SCE} upon immersion, which is typical for active zinc and reflecting corrosion of the zinc exposed at the rim of the drilled defect, as well as zinc extending a short distance in the annular region or crevice between the polymer and the steel at the defect perimeter. Within 1-4 days the OCP increased to ~-400mV_{SCE} , suggesting onset of very slow active dissolution or a tendency to passive behavior in that region.

Polarization Kinetics. In the following the results are reported as current per bar. Division of the current by the total exposed steel area per bar (~0.45 cm^2) would yield a corresponding nominal current density. However, its meaning would be limited considering the presence of undercoating corrosion and blistering, and that in the case of DCR metal dissolution may be concentrated in an annular region at the edge of the defect. Unless indicated otherwise the current values reported are the average terminal values from the last week of test.

For ECR in the +100mV_{SCE} polarization regime, small anodic currents (~0.02μA) per bar were measured in chloride-free solution and large anodic currents (in the order of 1 mA) were measured in chloride solution. As the OCP of ECR in chloride environment was ~-600mV_{SCE}, anodic behavior (anodic current in the order of 0.1 mA) was also observed in the -500mV_{SCE} regime.

Current measurements for DCR, in the +100, -500, and -1000 mV_{SCE} regimes, in both solutions showed initially high anodic reaction rates which indicate initial corrosion of the exposed zinc coating around the circumference of the defect sites. For the +100mV_{SCE} regime in chloride free SPS solution, anodic current stabilized after a few days to ~0.2 μA. This decrease indicates eventual passivation of the steel in chloride-free alkaline environment, and the onset of very slow dissolution of the zinc. In chloride containing SPS solution, the anodic current decreased but reached a high plateau (in the order of 0.1 mA) which was nevertheless much smaller than for ECR at the same +100mV_{SCE} polarization.

Cumulative anodic charge plots for ECR and DCR in the +100mV_{SCE} regime are shown in Figure 5. The large cumulative charge in chloride solution confirmed the effect of chlorides in strong anodic polarization to initiate corrosion but was significantly lower in DCR than ECR. The sharp increases in the anodic charge rate of ECR in chloride solution late in the exposure reflect incidents where anodic blistering and tearing had occurred on the coating. There was a lesser effect on DCR which may be associated with less accumulation of corrosion products in crevices when zinc was present. The cumulative anodic charge of ECR and DCR in chloride solution followed an approximately square root of time dependency, suggesting that corrosion deeper in crevices was transport limited. The relatively larger cumulative charge for DCR in chloride-free solution was consistent with the finite corrosion rate noted earlier.

In chloride-free solution, similar cathodic currents (2-3μA) were measured for ECR polarized to both -500 and -1000 mV_{SCE} (Figures 6-7) indicative of oxygen diffusion limitation (at least at the more negative potential). Similar cathodic currents were also measured for ECR polarized -1000 mV_{SCE} in chloride solution. For the DCR samples polarized -500 and -1000 mV_{SCE} in chloride and chloride free SPS solutions there was a cross-over from anodic behavior to cathodic behavior within the first couple of days. Similar cathodic currents (1-3 μA) were observed for these cathodically polarized bars indicative of oxygen diffusion limitation there as well.

Electrochemical Impedance Spectroscopy. Figure 8 shows equivalent circuits that were found to be adequate for analysis of EIS measurements of OCP specimens with a minimum of adjustable parameters. The circuit in Figure 8a was used for all cases except for ECR in SPS chloride solutions. Rs represents the solution resistance, Rp the polarization resistance and the constant phase element (CPE) with admittance term Yo and coefficient n accounts for interfacial charge storage. For ECR in SPS chloride solution (Figure 8b), a diffusional impedance element was added and separate branches used for the cathodic and anodic processes[17]. The parameter Ra_A represents the polarization resistance of the activation limited component of the anodic process. Rc_A represent the corresponding component of the cathodic process, and W represents the cathodic diffusional impedance. The nominal corrosion current for the simple system analog would be as shown in Eq. 1 where B is the Stern-Geary constant (assumed to be approximately 0.026 V).

$$I_{corr} = \frac{B}{Rp} \tag{1}$$

For ECR in SPS chloride solution, the nominal corrosion current was calculated with Eq. 2 where βa is the anodic Tafel slope assumed to be 0.12 V.

$$I_{corr} = \frac{1}{2.303}\frac{\beta a}{Ra_A} \tag{2}$$

EIS measurements are shown in Figure 9 for OCP specimens. The calculated nominal corrosion currents are shown in Figure 10. The diagrams were consistent with predominantly passive behavior of the steel in the chloride-free SPS solution, showing behavior dominated by capacitive behavior of the steel surface and a polarization resistance that was large for ECR indicating predominantly passive steel (Icorr~ ~0.01 μA). The polarization resistance was initially much smaller for DCR indicating early active zinc corrosion around defect locations; and increase as the system aged indicated the onset of a slower corrosion regime in agreement with the OCP observations, with Icorr~~0.1 μA. In chloride solution ECR had much smaller polarization resistance confirming visual and potential indications of corrosion activity (Icorr ~2 μA). In contrast, DCR showed comparable impedance evolution trends and apparent corrosion current both in chloride and chloride-free solutions paralleling the OCP evolution trends and in agreement with the absence of significant external corrosion products in either case.

Coating Disbondment

Coating disbondment data are shown in Figures 11-13. A notable feature of DCR was that the as-produced zinc layer had only moderate tensile strength (~13 MPa, Figure 13), consistent with the internal laminar interfaces present in the layered microstructure of thermally sprayed metal [18]. As a result, the interfacial stress in the peel-off tests normally used for ECR tend to cause some extent of cohesive failure of the zinc layer which is not representative of adhesion loss. Consequently, the as-received DCR behaved per the test procedures used here as if it had experienced coating disbondment, exhibiting a qualitative rating of 2 (Figure 11) and a disbondment radial length of ~3.5 mm in the peel off quantitative test (Figure 12). As expected, the corresponding as-received results for ECR were a rating of 4 and a radial length of zero. Pending future development of a specialized disbondment test procedure for DCR, the results reported here were interpreted in comparison to the values obtained for the respective as-received material conditions. It is also noted that the tests conducted here for both materials involved cathodic potentials of only -1V_{SCE}, exposures of at least one month duration and a highly alkaline pore water base solution. Thus, direct comparison with the results of standardized cathodic disbondment tests (as specified for example in ASTM A775 where a plain NaCl solution and -1.5 V_{SCE} exposure for 1 week is used) is not warranted.

As shown in Figure 11, the ECR qualitative adhesion rating showed distinct losses relative to the as-received material for all test conditions, especially for the chloride exposures. In contrast the rating for DCR decreased relative to the as-received condition notably only for the anodic polarization chloride exposure, consistent with the development of significant undercoating corrosion there. The quantitative radial disbondment results were more informative, showing distinct degradation for both materials compared with the as-received conditions. The greatest disbondment was observed, as expected, for the chloride tests, notably for the anodic polarization where undercoating corrosion was conspicuous for both materials. The ECR trends, including also significant disbondment at -1 V_{SCE}, were consistent with those reported in earlier investigations[2,19] . The DCR results were somewhat less potential- dependent than those for ECR, possibly because of the presence of a baseline value for the as-received material as noted above. Subtracting that value, the disbondment radial distance relative to the as-received condition was overall comparable to, or less than, that experienced by ECR.

The information from the coating pull-off tests (Figure 13) was limited for most ECR test conditions by the strength of the test dolly cyanoacrylate-epoxy bond, so that only a lower bound could be obtained for the epoxy-bar bond in most cases. With that qualification, for ECR coating pull-off strength remained high for bars in chloride-free SPS solution, comparable to the as-received state with the exception of bars polarized -1000 mV_{SCE}, consistent with the large disbondment radius and low adhesion level measured there. ECR pull-off strength in chloride solution was low where corrosion

products developed as well, as in the +100 and -500 mV_{SCE} cathodic polarization regimes. Pull-off strengths for DCR in chloride and chloride-free SPS solution as well as in the as-received state were similar (~13 MPa) due to the limited cohesive strength of the zinc layer noted above, with the exception of negligible pull-off strength measured for DCR polarized +100mV_{SCE} where external corrosion had occurred. In general, ECR and DCR pull-off strength results were consistent with qualitative coating adhesion level and disbondment radial distance results.

Physicochemical observations at defects and disbonded regions.

Figures 14-16 show examples of steel and zinc surface described in this section. Observations for chloride free are considered first. For these tests the pH of water retained upon removal from the tank in the exposed drilled defect cavities remained alkaline (pH 11 to >12) for both ECR and DCR. No moisture was found under disbonded regions of the coating for ECR or DCR at any of the polarization regimes. The steel surface of ECR remained bright with no indication of corrosion activity. The zinc layer in DCR exposed by peeling was bright but showed some discoloration.

For chloride tests, the pH of solution retained outside defect cavities remained alkaline too (pH >12) for both ECR and DCR. Figure 14 shows the external appearance of the drilled defects for ECR and DCR before peel off tests were conducted, displaying external corrosion product development in the conditions noticed earlier. Undercoating moisture was found in ECR tested at +100mV_{SCE}, -500mV_{SCE} and OCP, as well as for DCR at +100mV_{SCE}. There was acidification (pH 4-6) of undercoating moisture in ECR at +100mV_{SCE} and -500mV_{SCE}, and for DCR at +100mV_{SCE}. Small amounts of undercoating moisture were observed around some ECR OCP defects but its pH could not be reliably measured there. As shown in Figure 16, there was steel surface discoloration in the disbonded region of ECR at +100mV_{SCE}, -500mV_{SCE}, and OCP, but that region remained bright for the -1000mV_{SCE} ECR tests. As shown in Figure 15, the undercoating region of DCR polarized +100mV_{SCE} was clearly darkened on a region with radius ~9mm centered on defect sites where the zinc layer had been consumed. The DCR metal surface around the defect for OCP, -500, and -1000mV_{SCE} was bright with minor discoloration.

Figure 17 shows metallographic cross sections of the as-received DCR, and the after- exposure condition around the defect rim for the OCP chloride free tests as an illustration. The typical layered appearance and spatial thickness variation of the sprayed metal deposit is apparent, as are normal bubbles in the polymer layer. In the example shown approximately 50-100 μm of the Zn deposit have been radially consumed around the rim of the defect, a value typical of the OCP exposures of DCR in tests both with and without chlorides. Metallography of DCR exposed to +100 mV_{SCE} in chloride-free tests showed radial consumption in the 100-200 μm range. DCR specimens exposed to more negative regimes showed only vestigial Zn consumption.

Closing comments

In chloride-free solution and +100 mV_{SCE}, there was larger anodic cumulative charge in DCR than ECR, which can be attributed to zinc consumption in the former. At the end of the test the cumulative anodic charge for DCR was ~2 coulombs. Taking the average zinc layer thickness 28 μm and assuming equal rate of zinc consumption at each of the 8 defect sites, the Faradaic equivalent for divalent Zn would corresponds to ~80 μm radial consumption around the defect. That estimate is comparable to the Zn loss found metallographically. Estimates of Zn consumption from the nominal corrosion currents calculated by EIS for DCR in OCP tests both with and without chlorides (Figure 10) showed also rough agreement with the metallographic determination of Zn loss, which was smaller but still comparable to that at +100 mV_{SCE} in chloride free solutions. The cumulative charge and the EIS

data indicated that radial progression of Zn loss continued at a fractional exponent of time in chloride free +100 mV_{SCE} tests as well as all OCP tests. If those trends were to continue, very long times would be required for Zn consumption under OCP conditions to reach distances in the order of the bar diameter. Additional work is in progress toward quantitatively projecting Zn consumption trends.

The longevity of the Zn layer at the OCP is of importance if the absence of steel corrosion with chlorides in those conditions was due not only to the initial active period at -1.2 V_{SCE}, but also to long term lowering of the OCP by the Zn. In the initial active period the Zn exposed at the defect rim was likely activated by contact with the highly alkaline medium, which results in Zn dissolution in the form of zincate ions [20] by

$$Zn + 2\ OH^- = ZnO_2^{2-} + H^2 \quad (3)$$

That period was brief however, and it may be proposed that it ended when Zn consumption moved the reaction front deep enough into the annular space being created between the polymer and the base steel. At that point the reaction may become limited by transport of OH^- ions into the annulus, as well as by occlusion (and even partial passivation) by formation of Zn oxides/hydroxides if the local pH is lowered sufficiently. Zn corrosion did proceed afterwards at the previously noted slow rate, which is seemingly enough to lower the OCP to the ~-400 mV_{SCE} range. There is increasing evidence that under those conditions the corrosion threshold for corrosion initiation may be increased substantially compared to that of unpolarized passive steel [21]. Such cathodic prevention of steel may be responsible for the sustained absence of corrosion initiation at the OCP of steel in DCR. The ratio $[Cl^-]/[OH^-]$~2 used in these experiments is only just above the upper end of the range of values associated with corrosion initiation of bare steel at the pH of these solutions [22], but corrosion at crevices around organic coating defects may be expected to be initiated at markedly lower values [23]. Indeed, ECR corroded substantially under the same conditions in the creviced area surrounding the defects, as evidenced by the potential and impedance data as well as by direct observation. The effective threshold for corrosion initiation of DCR in the present media has not yet been established. It is noted that early chloride threshold estimates for DCR in concrete reported in Ref 12 were about one order of magnitude greater than those for plain uncoated carbon steel. Such results may reflect factors such as the relative amount of area available for corrosion initiation, in a given test period, for coated and uncoated materials. Instead, further tests in this program will continue to focus on the relative corrosion resistance of DCR and ECR.

The +100mV_{SCE} anodic polarization tests in chloride solutions represented an extreme bracket case which helped differentiating between ECR and DCR responses. Visual monitoring of ECR and DCR specimens revealed significant corrosion under these conditions, but the extent of corrosion product formation was significantly larger in ECR than DCR. Anodic blistering was more prevalent in ECR; blistering and subsequent external corrosion formation was observed on average 6 locations per bar away from intentional defects on ECR whereas only two spots with initial coating swelling was observed on DCR. Anodic current in ECR was approximately 5 times larger than DCR and is consistent with corrosion observations. Zinc corrosion products may have been more fluid than those in ECR facilitating escape and resulting in less swelling; moreover the amphoteric character of Zn may have assisted in developing less extreme acidic conditions in the DCR crevices than for ECR. It is noted however that differentiation between DCR and ECR under severe anodic conditions may be quite different in concrete, where the swelling will be strongly limited by surrounding solid matrix.

The early anodic behavior of DCR in both solutions measured in the -500 and -1000 mV_{SCE} regime[19] quickly transitioned to cathodic currents. However, the terminal cathodic currents in ECR and DCR in the tested polarization regimes were comparable with no indication greater tendency for

macrocell action in DCR. There was a slowdown in cathodic current with time for ECR and DCR in both solutions, which is consistent with oxygen transport limitation especially under the disbonded coating crevices. In the test defect configuration used here there is at the beginning of the test an ~40:1 exposed area of steel to zinc for DCR, which should only show a marginal effect in O_2 reduction rates compared to those on ECR. A more clear differentiation (likely lower oxygen reduction cathodic current for DCR) is expected if the defects on DCR did not go through to the steel but instead exposed primarily zinc. Test with such defect configuration are being implemented in continuing testing.

CONCLUSIONS

The following apply to Dual Coated Rebar (DCR) and Epoxy Coated Rebar (ECR) both with intentional defects of the same size drilled through the base steel and immersed in simulated concrete pore water solution:

- The polymer coating adhesion of DCR was found to be limited by the cohesive strength of the sprayed zinc layer. However, bond degradation of DCR relative to the as-received condition was comparable to, or less than, that experienced by ECR. This behavior was found for tests under both anodic and cathodic polarization and with and without the presence of chloride ions.

- Both DCR and ECR experienced severe corrosion under strong anodic polarization in simulated pore solution with chloride ions, but the extent of corrosion observed for DCR was significantly less than for ECR. This difference may be due in part to lesser accumulation of expansive corrosion products in the crevices surrounding the defects in DCR, with consequently less coating disruption than in the case of ECR .

- After a brief period of high activity, the open circuit potential (OCP) of DCR stabilized to ~-400 mV SCE both in the presence and absence of chloride ions. The exposed steel remained free of corrosion in either case. In contrast, ECR in the presence of chlorides developed more negative OCP and visible corrosion, confirmed by electrochemical measurements. The results suggest that corrosion mitigation at the OCP in DCR was due to galvanic coupling with corroding zinc exposed at the defect rim, which prevented corrosion initiation of the exposed steel at the chloride levels used in the tests.

- After the initial period of high activity, OCP consumption of the zinc exposed at the defect rim proceeded at a very low rate both in the presence or absence of chloride ions.

- In the absence of chloride ions and under medium to strong cathodic polarization, DCR showed cathodic current (and hence an ability to support corrosion macrocells with through-the-steel defects) no greater than that for ECR.

ACKNOWLEDGEMENTS

This investigation was supported by Gerdau Ameristeel. The opinions, findings, and conclusions expressed here are those of the authors and do not necessarily represent those of the funding organization. Acknowledgment is made to Adrienne Accardi, Keller Charles, Howard Fox, Carlyn Krapf, and Edward Lopez for their assistance in various phases of this research.

REFERENCES

1. Clear, K. Concrete International, Vol.14, No.5. pp.58-64, 1992.

2. Sagüés, A.A. et al. Final Report, "Corrosion of Epoxy-coated Rebar in Florida Bridges", WPI No. 0510603, Florida Department of Transportation, Tallahassee, FL, May, 1994. (Available online from Florida Department of Transportation).

3. Ramniceanu, A., Weyers, R., Riffle, J. and Sprinkel, M, ACI Mat. J. V. 105, p. 459, 2008.

4. Griffith, A. and Laylor, H.M. "Epoxy Coated Reinforcement Study." Final Report. Epoxy Coated Reinforcement Study, Project No.527. Oregon Department of Transportation, June 1999.

5. Fanous, F. and Wu, H. Journal of Bridge Engineering. Vol. 10, No.3, pp.255-261, 2005.

6. Darwin, A.B. and Scantlebury, J.D. Cement and Concrete Composites. Vol.24. pp.73-78, 2002.
7. Lau, K., Sagüés, A.A., and Powers, R.G. Corrosion/2007, Paper No.07306, NACE International, Houston, TX, 2007.

8. Lau, K., Sagüés, A.A., and Powers, R.G. Corrosion/2008, Paper No.08311, NACE International, Houston, TX, 2008.

9. Cui, F, Lawler, J., and Krauss, P. Corrosion/2007, Paper No.07286, Nace International, Houston, TX, 2007.

10. Nguyen, T. and Martin, J.W. JCT Research, Vol.1, no.2, pp.81-92, 2004.

11. Marquardt, A. Concrete International. Vol. 30, No. 9. pp.53-55, September 2008.

12. Clemeña, G.G. Interim Report, Investigation of the Resistance of Several New Metallic Reinforcing Bars to Chloride-Induced Corrosion in Concrete. Report No. VTRC 04-R7. Virginia Transportation Research Council, Charlottesville, VA, December 2003.

13. Darwin, D., Browning, J., Locke, C.E., Nguyen, T.V. Interim Report, Multiple Corrosion Protection Systems for Reinforced Concrete Bridge Components. Report No. FHWA-HRT-07-043. Office of Federal Highway Administration, McLean, VA, July 2007.

14. Darwin, D., Browning, J. 2008 Concrete Bridge Conference. Paper No. 101, National Concrete Bridge Council, Stokie, IL, 2008.

15. Vaca-Cortés, E., Lorenzo, M.A., Jirsa, J.O., Wheat, H.G., Carrasquillo, R.L. Adhesion Testing of Epoxy Coating. Report No. 1265-6. Texas Department of Transportation, TX, September 1998.

16. Sagüés, A.A. and Powers, R.G.,"Coating Disbondment in Epoxy-Coated Reinforcing Steel in Concrete - Field Observations", Corrosion/96, Paper No. 325, NACE International, Houston, 1996.

17. Sagüés, A.A., Corrosion, Vol. 44, p. 555, 1988.

18. Sagüés, A.A. and Powers, R.G., Corrosion, Vol. 52, p.508, 1996.

19. "Effect of Concrete Environment on the Corrosion Performance of Epoxy-Coated Reinforcing Steel", A. Sagüés and R. Powers, Paper No. 311, 16 pp., Corrosion/90, National Assoc. of Corr. Engs., Houston, 1990.

20. Pourbaix, M. Atlas of Electrochemical Equilibria in Aqueous Solution. NACE: Houston, 1974.

21 Presuel-Moreno, F.J., Sagüés, A.A., and Kranc, S.C. Corrosion, Vol. 61, p.428, 2005.

22. Li, L. and Sagüés, A.A., Corrosion, Vol. 57, p.19, 2001.

23. Sagüés, A.A., Li, L., and Pickering, H.W., Corrosion, Vol. 56, p.979, 2000.

Table 1. Solution constituents gram per 1L H_2O

	NaOH	KOH	$Ca(OH)_2$ †	NaCl	pH
SPS	3.7	10.5	2.1	-	13.3
SPS w/ NaCl	3.7	10.5	2.1	35 g	13

† Not fully dissolved in solution.

Table 2. Length of polarization test† (days)

	mV_{SCE}	ECR				DCR			
SPS	100	GN1A	41	GN1B	38	YN1A	37	YN1B	41
	-500	GN2A	41	GN2B	35	YN2A	37	YN2B	41
	-1000	GN3A	41	GN3B	35	YN3A	37	YN3B	35
	OCP	GN4A	41	GN4B	33	YN4A	37	YN4B	33
SPS with NaCl	100	GS1A	47	GS1B	53	YS1A	54	YS1B	46
	-500	GS2A	41	GS2B	52	YS2A	50	YS2B	46
	-1000	GS3A	40	GS3B	50	YS3A	49	YS3B	35
	OCP	GS4A	40	GS4B	49	YS4A	49	YS4B	41

† The table lists the time of exposure for the main test sequence. Additional results from supplemental OCP DCR samples are from the first ~50 days of exposure.

Table 3. Coating adhesion level scale

Adhesion Level Scale
1. Easily disbonded. Coating peels upwards during cutting. Total loss of adhesion to substrate.
2. Disbonded but small force required to to peel coating. Lever-arm motion with knife tip seperates coating from substrate.
3. Disbonded but force required to peel coating. Coating comes off substrate but with difficulty in cutting and some parts of coating remains adhered to surface.
4. Cannot be separated from steel substrate by prying or lifting motion.

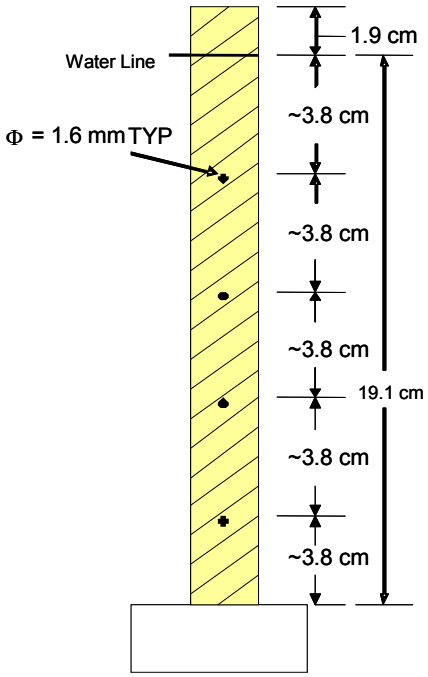

Figure 1. Schematic of bar sample and defect location.

Figure 2. Disbondment radius by knife test

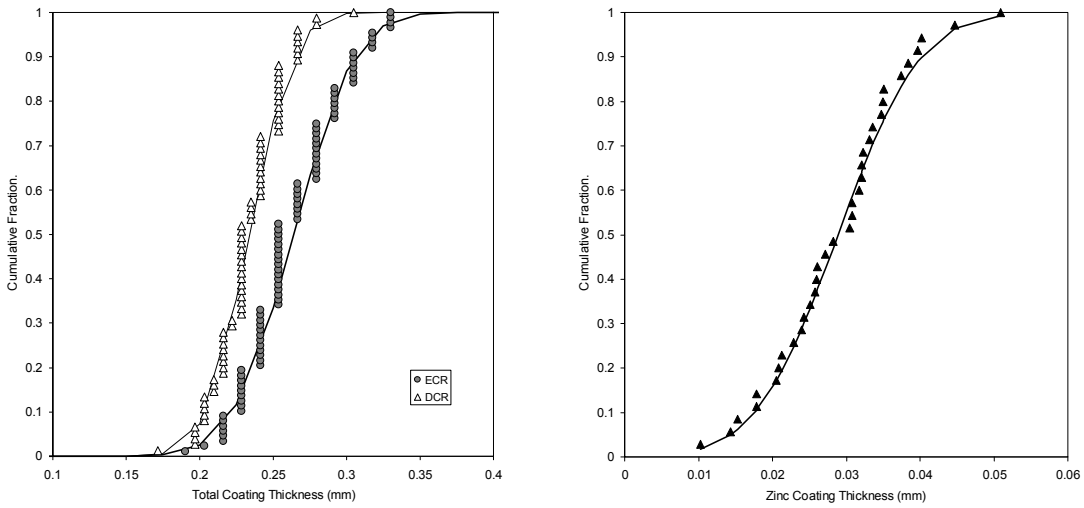

a) b)

Figure 3. Coating thickness. a) Total thickness; b) zinc coating

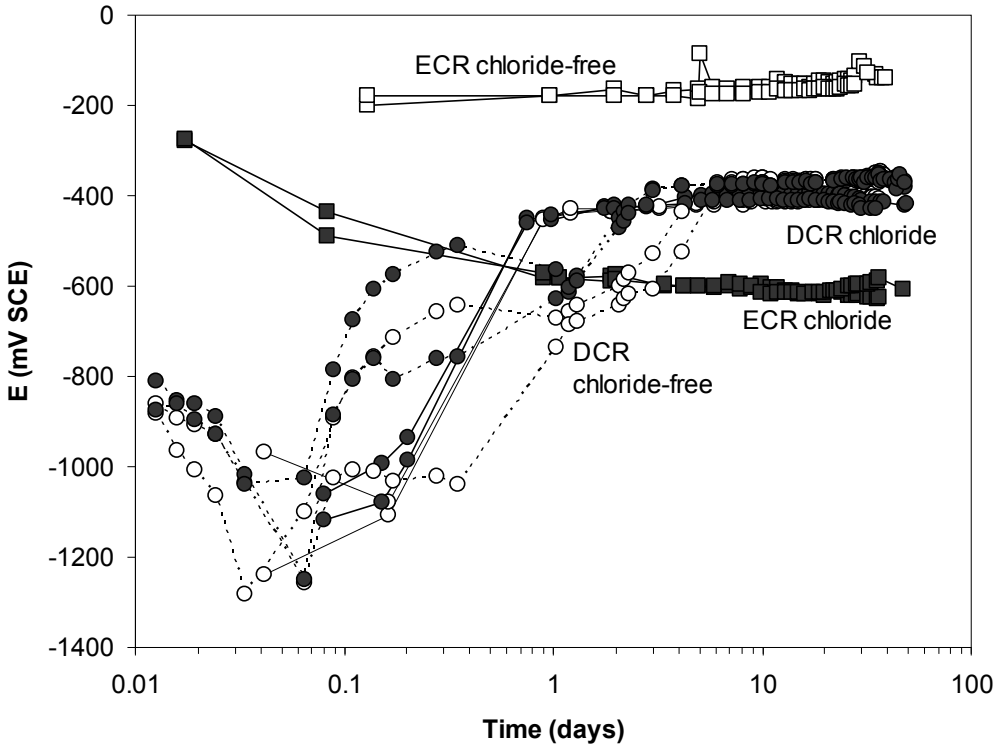

Figure 4. ECR and DCR open circuit potential. Square: ECR. Circle: DCR. Solid Line: Main sequence specimens. Dotted Line: Supplemental DCR specimens. White: SPS solution without NaCl. Grey: SPS solution with 3.5 wt% NaCl.

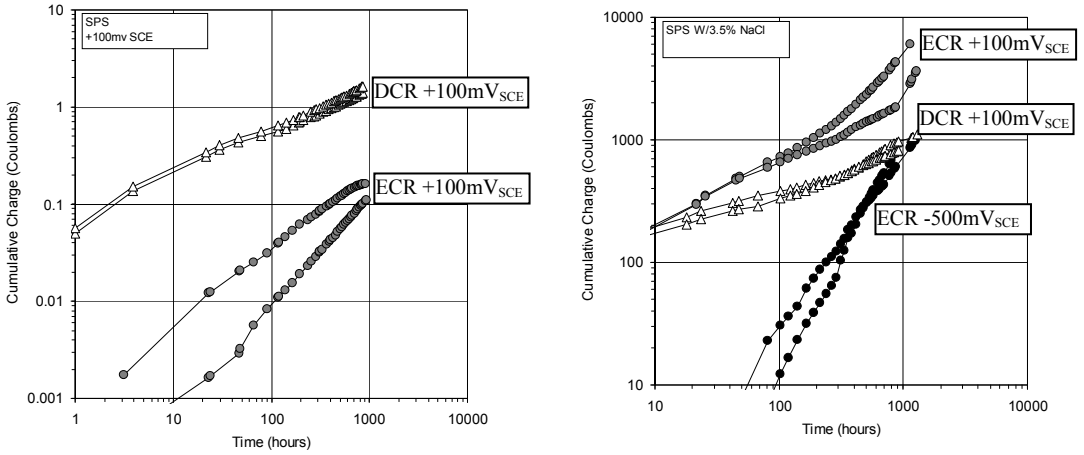

a) b)

Figure 5. Cumulative anodic charge for ECR and DCR in a) SPS solution and b) SPS solution with 3.5wt% NaCl addition. Circle: ECR. Triangle: DCR.

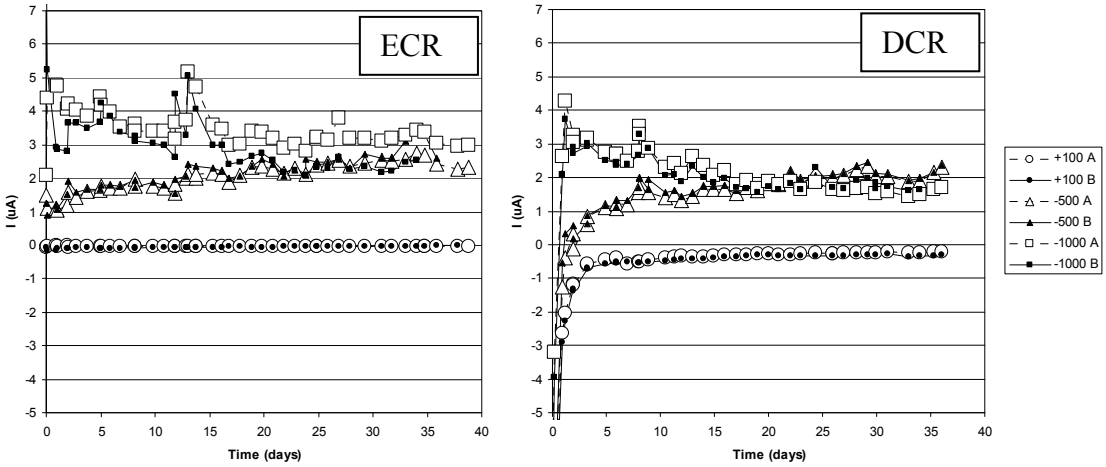

a) b)

Figure 6. Current measurements for a) ECR and b) DCR in chloride-free solution. Circle: +100mV$_{SCE}$. Triangle: -500mV$_{SCE}$. Square: -1000mV$_{SCE}$. Negative current represent anodic current. Positive current represent cathodic current.

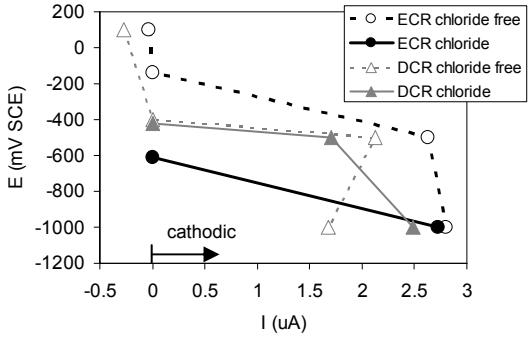

Figure 7. Cathodic current delivery at end of test.

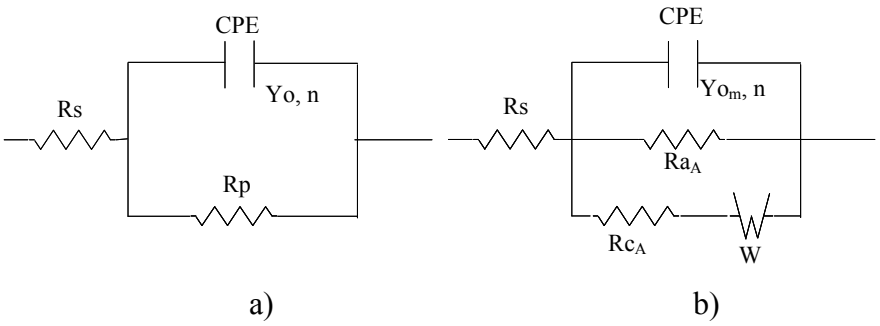

a) b)

Figure 8. EIS Equivalent Circuits

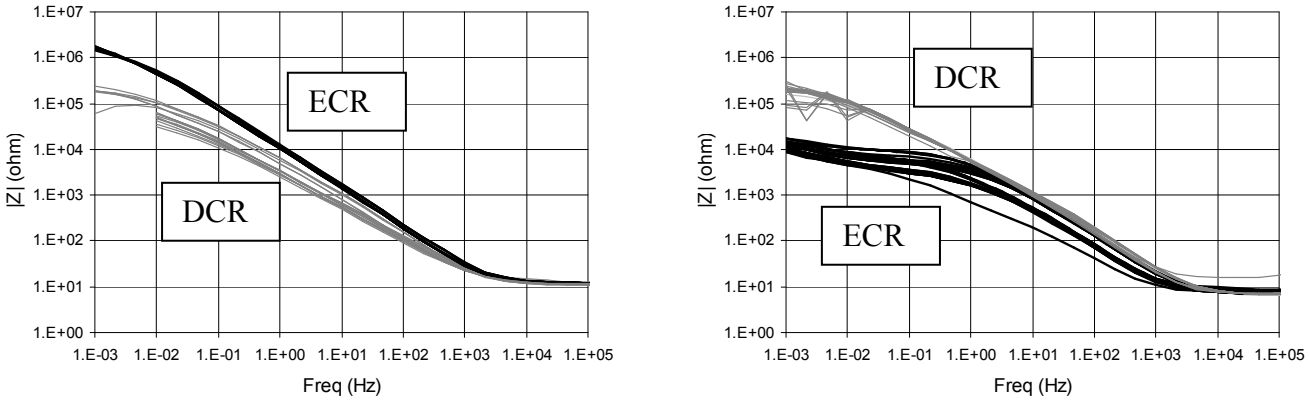

a) b)

Figure 9. Impedance Bode plots in a) SPS solution b) SPS solution with 3.5wt% NaCl.

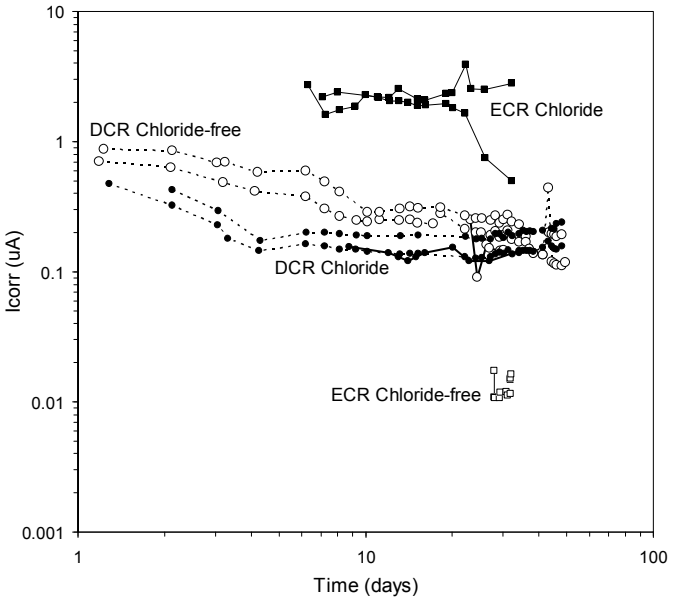

Figure 10. Nominal corrosion rates of ECR and DCR exposed in SPS solution with or without NaCl addition. Square: ECR. Circle: DCR. Solid Line: Main sequence specimens. Dotted Line: Supplemental DCR specimens. White: SPS solution without NaCl. Grey: SPS solution with 3.5 wt% NaCl.

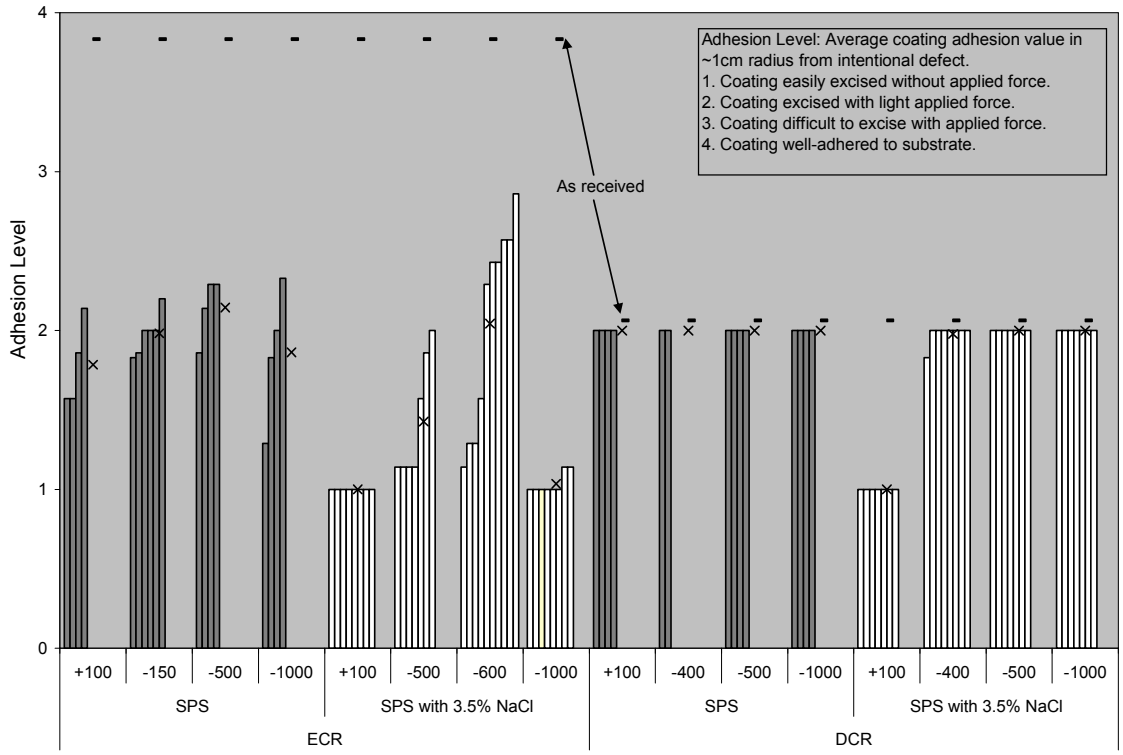

Figure 11. Epoxy coating adhesion level for ECR and DCR held at various potentiostatic regimes in SPS solution with or without NaCl additions. Averages for each condition indicated by X.

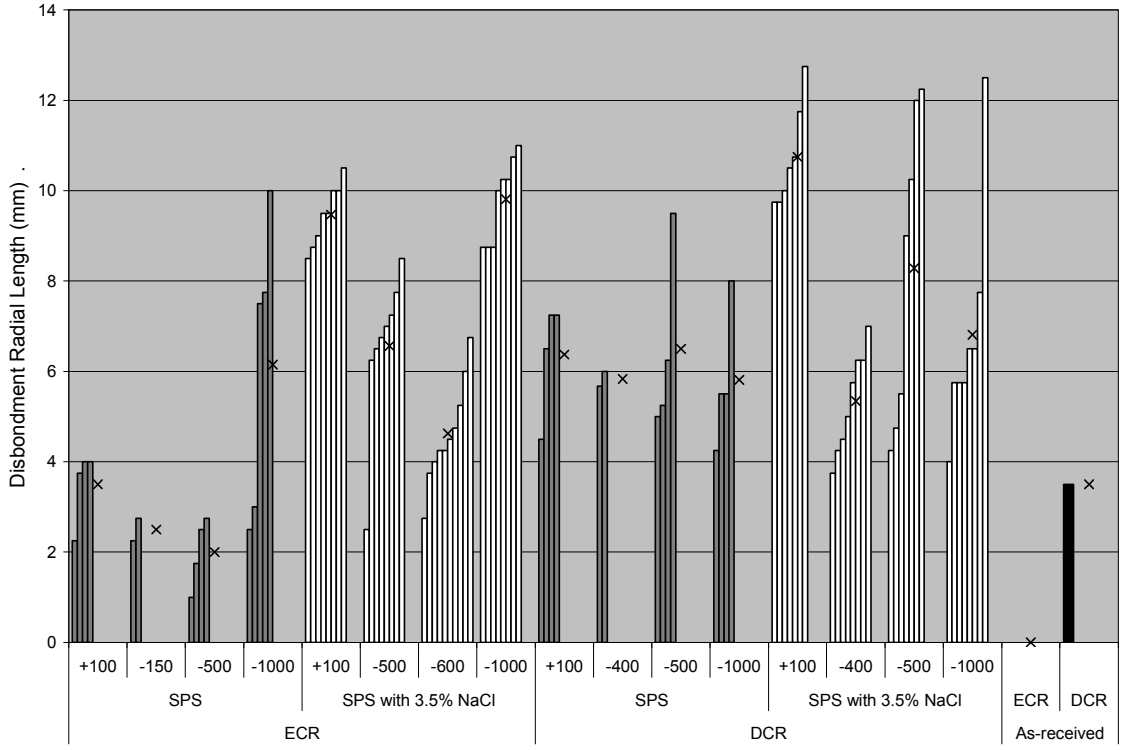

Figure 12. Epoxy coating disbondment radial length for ECR and DCR held at various potentiostatic regimes in SPS solution with or without NaCl additions. Averages for each condition indicated by X.

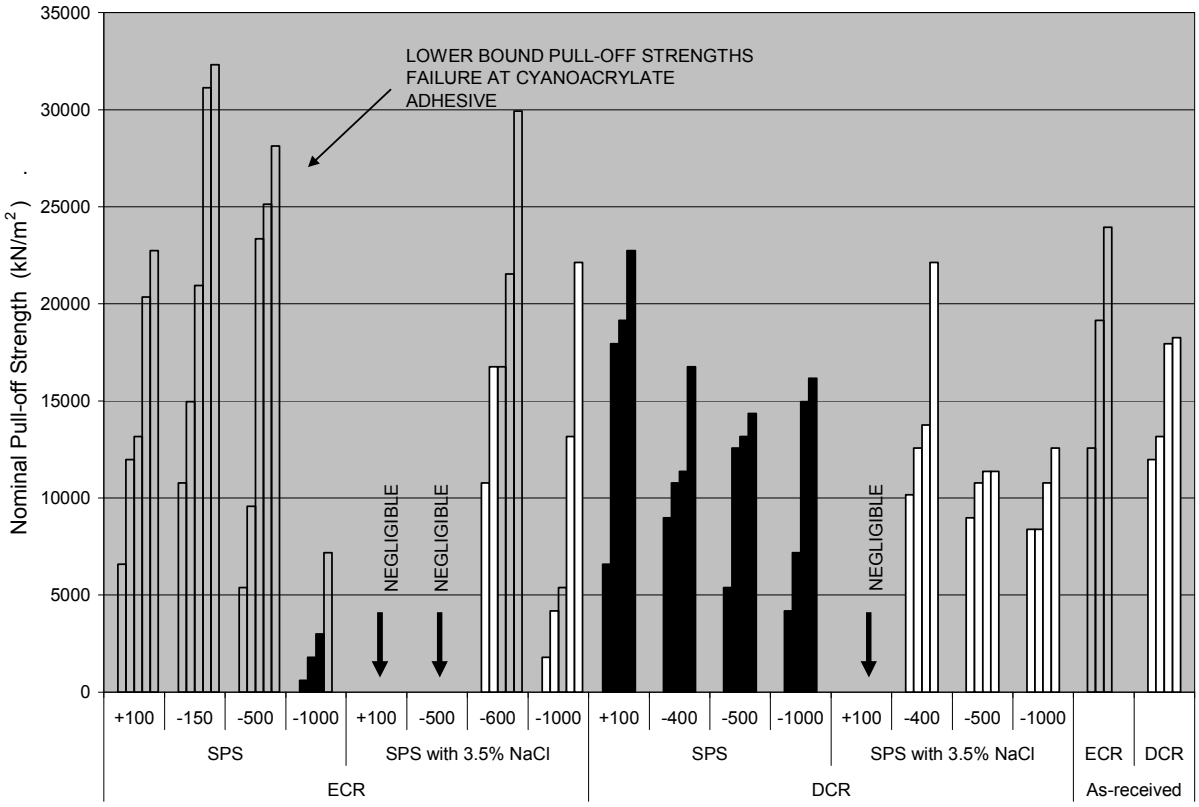

Figure 13. Epoxy coating pull-off strength for ECR and DCR held at various potentiostatic regimes in SPS solution with or without NaCl additions. Gray columns indicate tests where the cyanoacrylate bond to the test dolly failed before the coating-bar bond did, so the value reported is a lower bound of the latter.

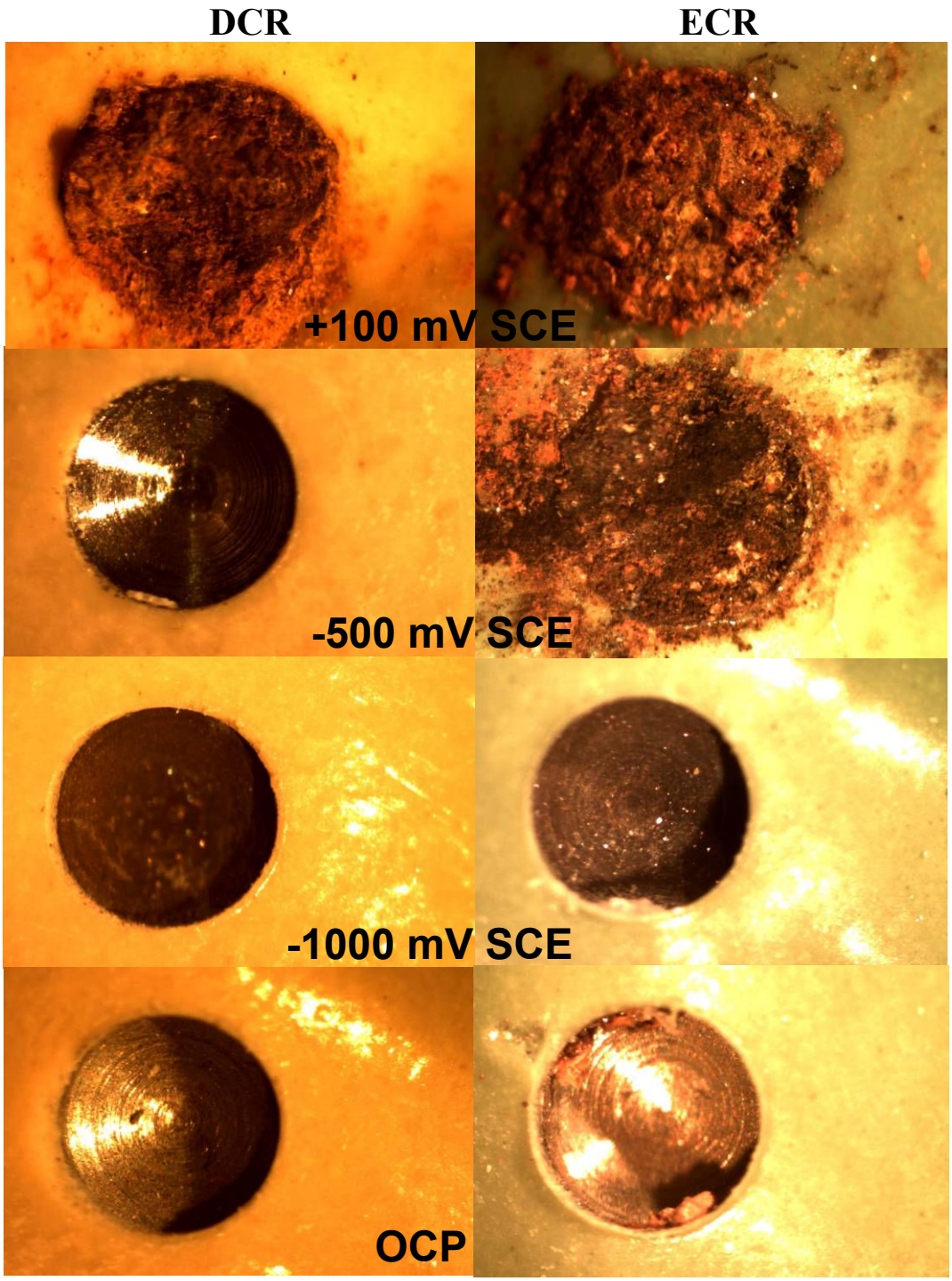

Figure 14. Coating defect sites after exposure in chloride SPS solution.

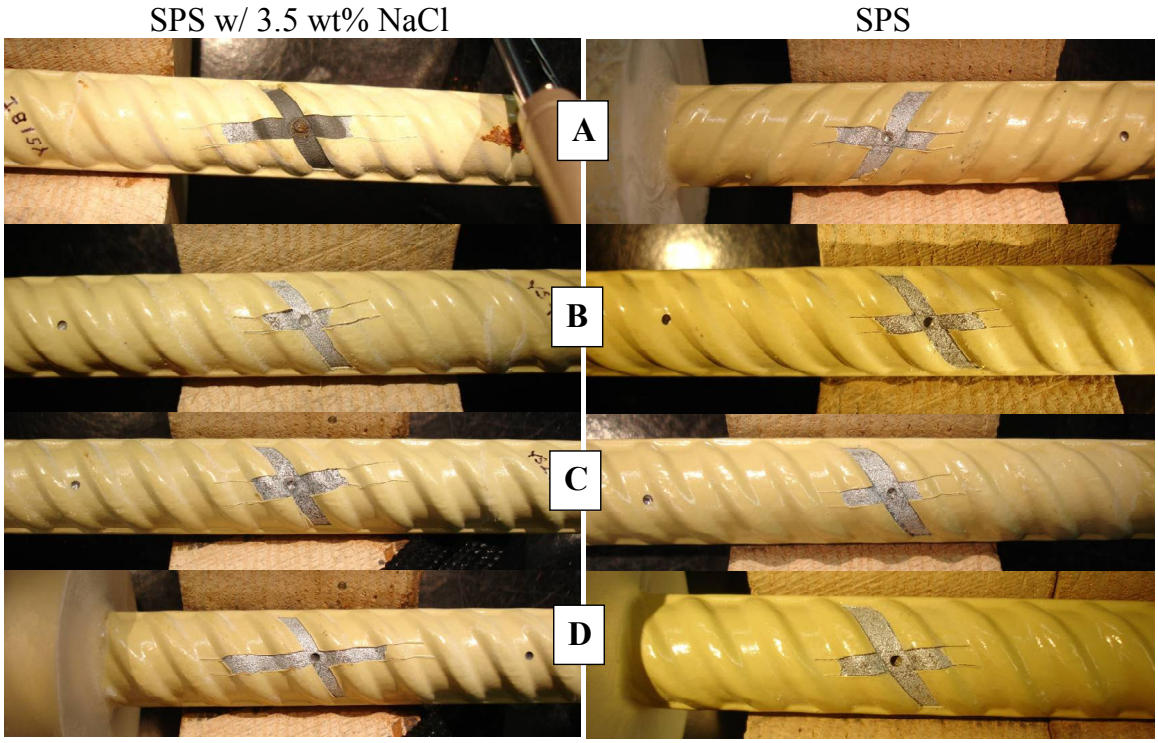

Figure 15. DCR zinc layer around defect site after exposure in SPS solution with and without 3.5wt% NaCl at A) +100mV SCE, B) OCP, C) -500mV SCE, D) -1000mV SCE

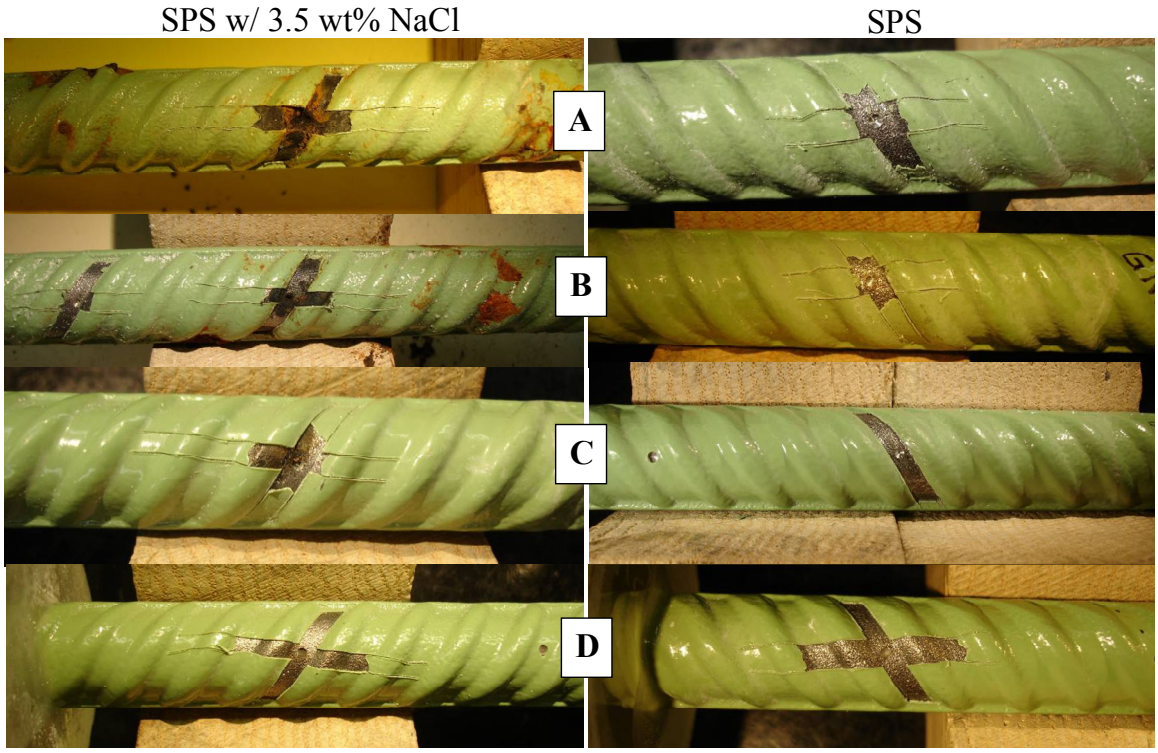

Figure 16. DCR steel surface around defect site after exposure in SPS solution with and without 3.5 wt% NaCl NaCl at A) +100mV SCE, B) -500mV SCE, C) OCP, D) -1000mV SCE.

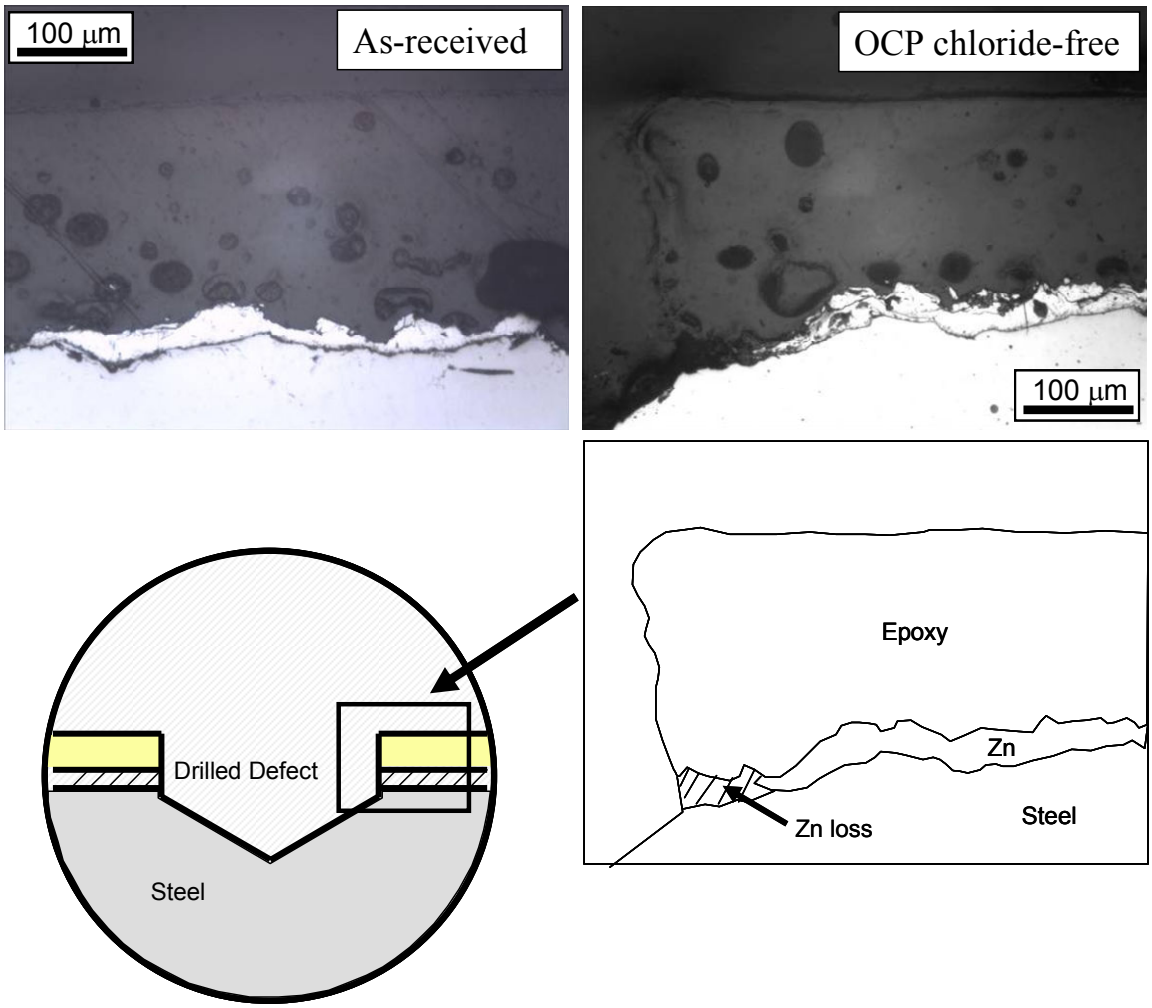

Figure 17. Metallographic cross section of DCR in the as-received condition and illustrating zinc consumption around the defect rim for the OCP chloride free tests.